Results in Engineering 27 (2025) 105918

Contents lists available at ScienceDirect

Results in Engineering

journal homepage: www.sciencedirect.com/journal/results-in-engineering

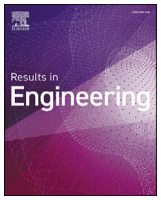

Research paper

Enhanced model predictive current framework for a PMSM powered by three-level NPC inverters with DC-link voltage self-balancing mechanisms

Kim-Anh Nguyen [a], L.D. Hieu [b], Viet-Tuan Pham [c], Van-Quang-Binh Ngo [c,*]

[a] Faculty of Electrical Engineering, The University of Danang - University of Science and Technology, Danang, Viet Nam
[b] School of Engineering and Technology, Hue University, Hue, Viet Nam
[c] Faculty of Physics, University of Education, Hue University, Hue, Viet Nam

ARTICLE INFO

Keywords:
Neutral point clamped inverter
Finite control set model predictive control
Capacitor voltage balancing
Permanent magnet synchronous motor
Processor-in-loop

ABSTRACT

This research presents an enhanced model predictive current control strategy for a three-level Neutral Point Clamped inverter driving a permanent magnet synchronous motor. The proposed new strategy significantly reduces computational complexity and balances the DC-bus capacitor voltages without weighting factors. Unlike conventional finite control set model predictive control, which requires exhaustive searches through all feasible switching conditions during iterative optimization, the proposed method streamlines a two-stage optimization procedure. In the initial stage, it utilizes the switching state of a P-type small vector. Medium voltage vectors are reconstructed from two suitable small vectors before the rolling optimization. Finally, the most effective switching signals are implemented in the 3L-NPC inverter by combining the best switching states identified in the optimization loop with the facilitated suggested self-balancing mechanisms for small vectors. The effectiveness of the suggested technique is validated via comprehensive comparative simulations and processor-in-loop experiments, executed under both stable and dynamic transitional conditions. The suggested approach achieves performance levels similar to traditional methods regarding settling time for speed, current ripple, and harmonic distortion of the current, all while decreasing the computational load by 30%. Compared to the prior method, capacitor voltage balancing is guaranteed under all operating conditions, particularly at low speeds. This result reduces stator current total harmonic distortion by 49.8% at 500 rpm due to the corrective of the medium voltage vector's impact.

1. Introduction

Permanent magnet synchronous motors (PMSMs) are extensively employed in electric vehicles and various industrial applications due to their remarkable efficiency, substantial torque, and significant power density [1–4]. Recently, the multilevel inverter has been recognized for its significant benefits over the established two-level configuration, including lower voltage stress, enhanced output voltage quality, reduced switching losses, and high power capacity [5,6]. These benefits are fulfilled by the three-level neutral point-clamped (3L-NPC) inverter, making it a highly suitable option for PMSM system applications requiring high power and high voltage [7–9].

In such applications, field-oriented control (FOC) and direct torque control (DTC) are the two predominant methodologies. FOC delivers rapid dynamic reactions and superior steady-state conditions via current and speed control loops with proportional-integral (PI) [10,11]. However, accurately identifying the motor's parameters poses a challenge due to the impact of diverse operating conditions, such as disturbances, temperature fluctuations, and frictional forces, which result in variations in these parameters. Conversely, DTC employs lookup tables to generate switching signals without relying on modulation technique, allowing for a quick response, but typically resulting in significant torque ripple and elevated switching frequencies [12,13]. The use of model predictive control (MPC) in PMSM drives has significantly increased in

Abbreviations: FOC, Field oriented control; CCS-MPC, Continuous control set model predictive control; DTC, Direct torque control; DSP, Digital signal processor; FCS-MPC, Finite control set model predictive control; FFT, Fast Fourier Transform; NP, Neutral Point; NPC, Neutral Point Clamped; PI, Proportional-integral controller; PIL, Processor-in-loop; PMSM, Permanent magnet synchronous motor; RMSE, Root mean square percentage error; THD, Total harmonic distortion; 3L-NPC, Three-level Neutral Point Clamped.

* Corresponding author.
E-mail addresses: nkanh@dut.udn.vn (K.-A. Nguyen), ledinhhieu@hueuni.edu.vn (L.D. Hieu), pvtuan@hueuni.edu.vn (V.-T. Pham), nvqbinh@hueuni.edu.vn (V.-Q.-B. Ngo).

https://doi.org/10.1016/j.rineng.2025.105918
Received 18 April 2025; Received in revised form 9 June 2025; Accepted 21 June 2025
Available online 27 June 2025

Nomenclature

ω_e, ω_m	Electrical angular speed and rotor speed.
ψ_m	Rotor flux linkage.
θ	Electrical angle associated with the rotor.
C_1, C_2	DC-link capacitors.
i_{sa}, i_{sb}, i_{sc}	Three-phase stator current.
i_{sd}, i_{sq}	Stator current in dq-axis.
L_s	Phase inductance.
R_s	Phase resistance.
S_x	Switching status of inverter with $x \in \{a, b, c\}$.
T_e	Electromagnetic torque.
T_s	Sampling time.
u_o	Neutral-point voltage.
u_{sd}, u_{sq}	Stator voltage in dq-axis.
u_{xo}	Inverter phase voltage with $x \in \{a, b, c\}$.
V_{dc}	DC-link voltage.

Superscripts

$*$	Reference value.

Subscripts

d, q	d, q axis.
s	Stator.

recent years owing to its intuitive framework, excellent dynamic performance, and flexible multi-objective control capabilities [14–16]. This advancement has been largely supported by the accelerated evolution of digital signal processors, which enable efficient real-time implementation. MPC is categorized into two main types according to its control input: continuous control set model predictive control (CCS-MPC) and finite control set model predictive control (FCS-MPC). The CCS-MPC approach generates a continuous reference of voltage through the resolution of an optimization issue [15–17]. A significant challenge, however, lies in the high computational burden associated with addressing the quadratic programming problem at each sampling period, especially when taking into account constraints and nonlinearities. In contrast, the FCS-MPC approach employs a comprehensive method to identify the most suitable control variable from a limited set of discrete nature switching signals. Furthermore, the evaluation function is capable of effectively addressing non-linear constraints such as current, switching frequency, and capacitor voltage balancing [14,16,18].

FCS-MPC can be categorized based on the kind of predicted variable, including predictive current control [3,19,20], predictive torque control [7,9], predictive speed control [1,18,21], and predictive flux control [22]. Voltage imbalance in the DC-bus capacitors of 3L-NPC inverters adversely affects output quality, shortens the lifespan of the capacitors, and exposes switching devices to a heightened risk of failure due to differing voltage stresses. When implementing conventional FCS-MPC for PMSMs driven by a 3L-NPC inverter, the neutral-point (NP) voltage component must be incorporated into the cost function. This integration allows the controller to achieve multi-objective optimization, simultaneously managing stator current, torque, flux linkage, and NP voltage balance. Consequently, fine-tuning various weighting factors is imperative for achieving satisfactory control performance. Various alternative strategies focus on the weighting factor design by employing metaheuristic optimization technique, fuzzy logic, and artificial neural networks. However, accurately determining the adjustment of the numerous weighting coefficients is intricate, primarily depending on practical experience, and the design process is complex, leading to high computational demands. To solve the challenges associated with the two-level inverter, one can combine the electromagnetic torque and the stator flux into a single torque or a flux term [23,24]. Another approach involves merging the torque and flux elements into a stator voltage through the application of the deadbeat technique [15,25,26]. However, when these strategies are extended to 3L-NPC inverters, the NP voltage cannot be integrated with the other variables within the optimization criterion.

To eradicate the need for selecting an adjustment element for NP voltage control, several strategies employ the nearest three-vector approach. This method modifies the application timing of duplicative small vectors to maintain a mean current of zero via the NP during each sampling period [19,27]. However, these approaches may prove ineffective in scenarios with a high modulation index or a significant power factor, leading to compromised control performance. A new approach has been proposed that combines virtual vector space modulation with model predictive control for current or torque in 3L-NPC inverters [8,9,20,28,29]. This method aims to recombine small and medium vectors to reduce the impact of medium vectors on the imbalance of DC-link capacitor voltages under various operating conditions. Nonetheless, this technique requires complex trigonometric computations to accurately determine the precise sector or region of the inverter voltage vector within the space vector diagram. Additionally, it involves intensive dwell time calculations to accurately allocate the duration of switching states, ensuring the proper synthesis of the desired output voltage through the optimal distribution of the switching signals. A major challenge encountered by FCS-MPC in real-world applications is the substantial computational load associated with multilevel inverters. This arises from the need to thoroughly evaluate all possible combinations of switching control gates during the online computation phase. Consequently, this results in longer execution times, which require extended control cycles and adversely affect control performance. In [30,31], a novel approach is proposed for implementing 3L-NPC inverters, beginning with the calculation of the reference voltage vector. This vector is then straight assess with available voltage vectors in roll optimization. Their method significantly reduces the iteration time needed to forecast control objectives related to voltage vectors, thereby decreasing computational effort. However, the need to evaluate multiple redundant switching states introduces considerable computational complexity, limiting the practicality of this approach in certain scenarios.

To address the aforementioned challenges, our study presents an enhanced model predictive current control approach for a 3L-NPC inverter-fed PMSMs system. This approach eliminates the need for tuning weighting factors and enriches control performance, particularly under significant NP voltage imbalance caused by small and medium vectors. A predictive model is utilized to forecast the stator current derived from the inverter operating states and the observed control variable measurements. The control goals, including rotor speed regulation and NP voltage balance, are achieved through a defined cost function implemented in two phases. During the initial phase, the recommended approach employs the switching circumstances of a P-type small vector, thus bypassing the necessity for two redundant small vectors. Additionally, medium voltage vectors are reconstructed using two appropriate small vectors to rectify the imbalance in the DC-bus capacitor voltages. This approach minimizes the feasible voltage vectors for 3L-NPC inverters, lowering their total from 27 to 19, which aids in roll optimization. In the final phase, optimal switching signals are executed in the 3L-NPC inverters by integrating the most effective switching conditions from the optimization loop with the proposed DC-link voltage balancing for small vectors. Compared to conventional FCS-MPC [18] and earlier approaches [19], the proposed method significantly reduces computational complexity, eliminates the need for selecting a weighting factor, and reliably maintains neutral-point voltage balance under all operating conditions. This is especially effective in challenging scenarios, such as high modulation indices and low-speed operations. Table 1 provides

Table 1
Control strategies for PMSM supplied by 3L-NPC inverters.

Control methods	Advantages	Drawbacks
FOC	Acceptable performance	Low dynamic response Accurate machine parameters Complex modulation
DTC	Fast dynamic response Not modulation	High sampling frequency Significant torque ripple
CCS-MPC	High performance Fast dynamic response Easily constraint inclusion	Complex optimization for nonlinear system Complex modulation
Conventional FCS-MPC	High performance Fast dynamic response Easily constraint inclusion Simple optimization Not modulation	High computational burden Weighting factor selection
Previous FCS-MPC [19]	High performance Fast dynamic response Easily constraint inclusion Simple optimization Not modulation	Neutral-point voltage imbalance at high modulation indices and low speed
Suggested FCS-MPC [28]	High performance Fast dynamic response Easily constraint inclusion Simple optimization	Sector and dwell-time calculation via complex trigonometry
Proposed approach	High performance Fast dynamic response Easily constraint inclusion Simple optimization Not modulation	

a summary of the control strategies for PMSM powered by 3L-NPC inverters. This paper emphasizes several key advancements, which consist of:

- The offered strategy achieves NP voltage balancing by integrating a simplified algorithm that selects the proper switching combination from the redundant small vectors, along with suitable reconstruction of the amplitudes of the medium vectors. This approach eliminates the need for weighting factors, thereby reducing control complexity and avoiding the challenging task of tuning multiple weighting parameters. The NP voltages exhibited by the suggested method demonstrate a resemblance to those of the conventional FCS-MPC [18] under all operating conditions. However, unlike the prior technique [19], it fails to guarantee the balance of the DC-link voltage in specific circumstances due to the influence of medium vectors, such as low-speed conditions and high modulation indices.
- The strategy put forward results in a computational load reduction of approximately 30% relative to conventional FCS-MPC. This improvement is achieved by eliminating the need to predict NP voltage and by minimizing the number of stator current predictions and cost function evaluations. The insights gained from this research may facilitate the establishment of a viable control framework, making use of a cost-effective platform that operates with a minimized sampling interval.
- The proposed strategy delivers comparable performance to conventional FCS-MPC during both dynamic and steady-state conditions, demonstrating similar settling time for speed, current ripple, and total harmonic distortion (THD) of the stator current. Compared to the prior method outlined in [19], the THD of stator current in the proposed approach has been reduced by 49.8%, decreasing from 2.27% to 1.14% at 500 rpm. Particularly, the DC-link capacitor voltages are unbalanced due to the effects of the medium voltage vector.

This paper will be presented in the following structure: Section 2 introduces the system configuration and dynamic model of the 3L-NPC inverter-fed PMSM. Section 3 outlines the offered streamlined model predictive current control scheme, which incorporates self-balancing mechanisms of the DC-link capacitor voltages. Section 4 provides simulation results, comparative analysis, and discussion. To conclude, Section 5 presents a summary of the significant findings discussed throughout the paper.

Table 2
The diverse switching configurations of 3L-NPC inverters $x \in \{a, b, c\}$.

States	Switching pulses				Inverter voltage
S_x	S_{x1}	S_{x2}	S_{x3}	S_{x3}	u_{xo}
$[P]$	1	1	0	0	$V_{dc}/2$
$[O]$	0	1	1	0	0
$[N]$	0	0	1	1	$-V_{dc}/2$

2. The configuration and mathematical framework of the system's topology

A fundamental configuration of the PMSM supplied by three-level NPC inverters is depicted in Fig. 1. Each phase leg of the NPC inverter features four semiconductor switches and two clamping diodes. A split DC-link capacitor that divides the DC voltage into two equal halves, creating the neutral point (o). The functionality of the 3L-NPC inverters is defined by three specific switching states: [P], [O], and [N]. In the [P] status, both S_{x1} and S_{x2} switches are activated to "ON", producing an inverter terminal voltage $u_{xo} = V_{dc}/2$. In contrast, the [N] status reflects that lower two switches S_{x3} and S_{x4} are activated to "ON", resulting in a terminal voltage u_{xo} of $-V_{dc}/2$. The switching status designated as [O] indicates that the middle switches S_{x2} and S_{x3} are engaged in the "ON" state, causing u_{xo} being held at zero through the action of the clamping diodes. The activation of either of the two clamping diodes is contingent upon the direction of the current. Table 2 delineates the summary of the status changes induced by the inverter.

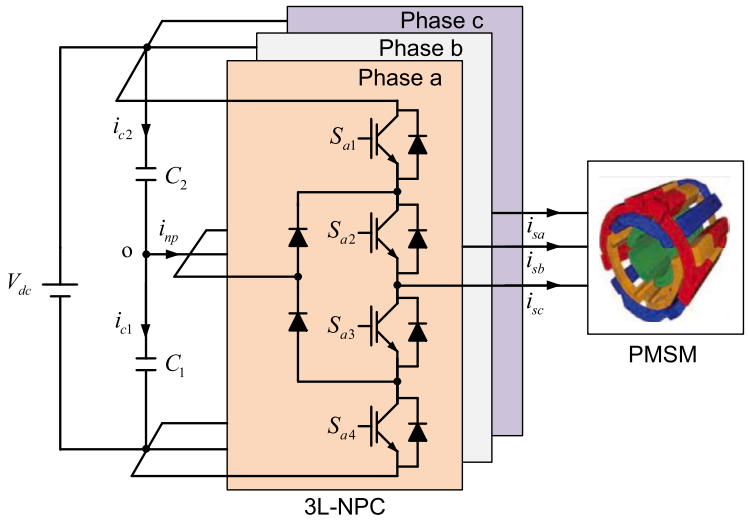

Fig. 1. Structure of the PMSM powered by 3L-NPC inverters.

Given that the equilibrium of capacitor voltages is assured, the inverter phase voltage, denoted as u_{xo}, concerning the neutral point can be expressed in a facilitated form as follows:

$$u_{xo} = \frac{S_x V_{dc}}{2}, \tag{1}$$

where V_{dc} signifies the DC-link voltage. The switching status is denoted by S_x, with S_x taking values from the set $\{-1, 0, 1\}$. These values are associated with the switching condition [P], [O], and [N], as depicted in Table 2.

Assuming a steady DC-bus voltage and the equality of capacitances ($C_1 = C_2 = C_{dc}$), the instantaneous NP voltage (u_o) can be characterized by the inverter operating states and the stator currents as:

$$\begin{aligned}\frac{du_o}{dt} &= \frac{d\left(u_{c1} - u_{c2}\right)}{dt} = -\frac{1}{C_{dc}} i_{np} \\ &= -\frac{1}{C_{dc}}\left((1 - |S_a|)i_{sa} + (1 - |S_b|)i_{sb} + (1 - |S_c|)i_{sc}\right).\end{aligned} \tag{2}$$

The representation of voltage equations for PMSM in the rotating coordinate frame, identified as the dq-axis, is provided as follows:

$$\begin{aligned}u_{sd} &= R_s i_{sd} + L_d \frac{di_{sd}}{dt} - \omega_e L_q i_{sq}, \\ u_{sq} &= R_s i_{sq} + L_q \frac{di_{sq}}{dt} + \omega_e L_d i_{sd} + \omega_e \psi_m,\end{aligned} \tag{3}$$

where $\omega_e = p\omega_m$ denotes the electrical angular speed, with ω_m representing the rotor speed and p indicating the number of pole pairs. The variables R_s, L_s, and ψ_m correspond to the phase resistance, inductance ($L_d = L_q = L_s$ for surface-mounted PMSM), and rotor flux linkage, respectively.

By varying the stator current in the d-axis, one can effectively control the electromagnetic torque:

$$T_e = \frac{3}{2} p \psi_m i_{sq}. \tag{4}$$

The stator current is determined from equation (3) as demonstrated in the following:

$$\begin{aligned}\frac{di_{sd}}{dt} &= \frac{u_{sd}}{L_s} - \frac{R_s}{L_s} i_{sd} + \omega_e i_{sq}, \\ \frac{di_{sq}}{dt} &= \frac{u_{sq}}{L_s} - \frac{R_s}{L_s} i_{sq} - \omega_e i_{sd} - \frac{\omega_e}{L_s}\psi_m,\end{aligned} \tag{5}$$

where the stator voltages, represented by u_{sd} and u_{sq} in the synchronous reference frame, can be established through the Park-transformation as:

$$\begin{bmatrix} u_{sd} \\ u_{sq} \\ u_{s0} \end{bmatrix} = [P] \begin{bmatrix} u_{sa} \\ u_{sb} \\ u_{sc} \end{bmatrix}, [P] = \frac{2}{3} \begin{bmatrix} \cos(\theta) & \cos\left(\theta - \frac{2\pi}{3}\right) & \cos\left(\theta + \frac{2\pi}{3}\right) \\ \sin(\theta) & \sin\left(\theta - \frac{2\pi}{3}\right) & \sin\left(\theta + \frac{2\pi}{3}\right) \\ \frac{1}{2} & \frac{1}{2} & \frac{1}{2} \end{bmatrix}, \tag{6}$$

where θ represents the electrical angle associated with the rotor.

Furthermore, the stator voltage pertinent to the PMSM aligns with the output voltage of the 3L-NPC inverter, as illustrated in Fig. 1. This voltage can be computed by considering the inverter operating states and the DC-link voltages, as described in the subsequent equations:

$$\begin{aligned}u_{sa} &= \frac{V_{dc}}{6}\left(2S_a - S_b - S_c\right), \\ u_{sb} &= \frac{V_{dc}}{6}\left(2S_b - S_a - S_c\right), \\ u_{sc} &= \frac{V_{dc}}{6}\left(2S_c - S_a - S_b\right).\end{aligned} \tag{7}$$

Employing the first-order forward Euler technique for the discrete approximation of equations (2) and (5) across a sampling period T_s results in the discrete-time formulation of the relevant model:

$$\begin{aligned}i_{sd}(k+1) &= \left(1 - \frac{R_s T_s}{L_s}\right) i_{sd}(k) + T_s \omega_e(k) i_{sq}(k) + \frac{T_s}{L_s} u_{sd}(k), \\ i_{sq}(k+1) &= \left(1 - \frac{R_s T_s}{L_s}\right) i_{sq}(k) - T_s \omega_e(k) i_{sd}(k) + \frac{T_s}{L_s} u_{sq}(k) \\ &\quad - \frac{T_s}{L_s}\psi_m \omega_e(k), \\ u_o(k+1) &= u_o(k) - \frac{T_s}{C_{dc}}\left((1 - |S_a(k)|)i_{sa}(k) + (1 - |S_b(k)|)i_{sb}(k)\right) \\ &\quad - \frac{T_s}{C_{dc}}(1 - |S_c(k)|)i_{sc}(k).\end{aligned} \tag{8}$$

Within practical applications, it is crucial to address the issue of calculation delay compensation. An effective strategy for mitigating this delay is to leverage the state observed at the kth instant to estimate the state at the $(k+1)$th instant, and then use this estimation to identify the optimal switching status for the $(k+1)$th instant. In this scenario, the stator currents and the NP voltage can be derived from the best inverter operating states at the prior sampling instant, along with system measurements and the model. Subsequently, the anticipated values at $k+2$ are forecasted based on the approximate values at $k+1$ and all switching status of the 3L-NPC inverters as:

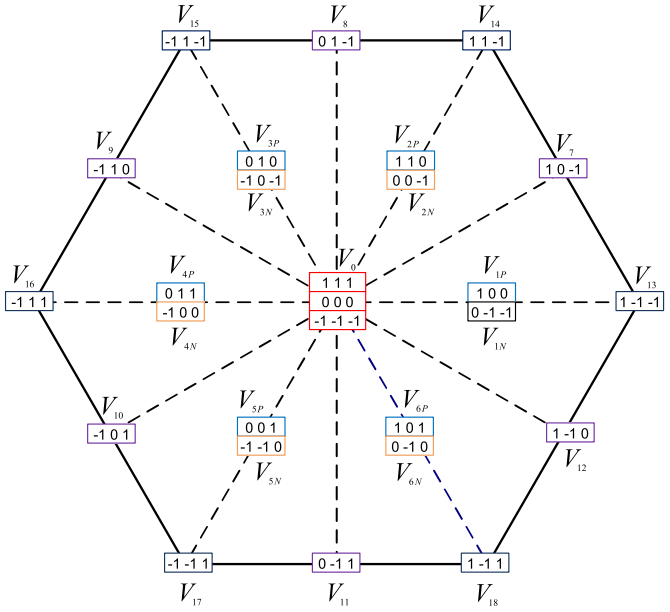

Fig. 2. Space vector representation of 3L-NPC.

$$
\begin{aligned}
i_{sd}(k+2) &= \left(1-\frac{R_sT_s}{L_s}\right) i_{sd}(k+1) + T_s\omega_e(k+1)i_{sq}(k+1) \\
&\quad + \frac{T_s}{L_s}u_{sd}(k+1), \\
i_{sq}(k+2) &= \left(1-\frac{R_sT_s}{L_s}\right) i_{sq}(k+1) - T_s\omega_e(k+1)i_{sd}(k+1) \\
&\quad + \frac{T_s}{L_s}u_{sq}(k+1) - \frac{T_s}{L_s}\psi_m\omega_e(k+1), \\
u_o(k+2) &= u_o(k+1) - \frac{T_s}{C_{dc}}\left(1-|S_a(k+1)|\right) i_{sa}(k+1) \\
&\quad - \frac{T_s}{C_{dc}}\Big((1-|S_b(k+1)|)i_{sb}(k+1) \\
&\quad + (1-|S_c(k+1)|)i_{sc}(k+1)\Big).
\end{aligned} \tag{9}
$$

3. Advanced structure for a PMSM utilizing three-level NPC with mechanisms for self-balancing voltage

This study focused on monitoring rotor speed with a quick dynamic response, reduced steady-state error, and maintaining capacitor voltage balance. To achieve these goals, conventional FCS-MPC methodologies for PMSM implement a cascaded design that features an external speed control based on a PI controller and a predictive controller for the inner stator current. The appropriate cost function that accounts for the compensation of computational delays can be formulated as follows [14,16]:

$$
\begin{aligned}
g(u_{k+1}) &= \left\|i^*_{sd}(k+2) - i_{sd}(k+2)\right\|^2 + \left\|i^*_{sq}(k+2) - i_{sq}(k+2)\right\|^2 \\
&\quad + \lambda_c \left\|u_o(k+2)\right\|^2,
\end{aligned} \tag{10}
$$

$i^*_{sd}(k+2)$ and $i^*_{sq}(k+2)$ indicate the desired stator current in the dq axis at the time instance denoted by $k+2$. The factor λ_c is a weighting parameter that facilitates the attainment of satisfactory performance in the balance of capacitor voltages.

The future estimation of stator currents can be achieved through the application of the second-order Lagrange extrapolation procedure:

$$
\begin{aligned}
i^*_{sd}(k+2) &= 6i^*_{sd}(k) - 8i^*_{sd}(k-1) + 3i^*_{sd}(k-2), \\
i^*_{sq}(k+2) &= 6i^*_{sq}(k) - 8i^*_{sq}(k-1) + 3i^*_{sq}(k-2).
\end{aligned} \tag{11}
$$

Table 3
Impact of NP current on medium and small vector classifications.

Inverter vector categories	Feasible voltage vectors	Neutral-point current
Medium vector	V_7	i_{sb}
	V_8	i_{sa}
	V_9	i_{sc}
	V_{10}	i_{sb}
	V_{11}	i_{sa}
	V_{12}	i_{sc}
P-type small vector	V_{1P}	$-i_{sa}$
	V_{2P}	i_{sc}
	V_{3P}	$-i_{sb}$
	V_{4P}	i_{sa}
	V_{5P}	$-i_{sc}$
	V_{6P}	i_{sb}
N-type small vector	V_{1N}	i_{sa}
	V_{2N}	$-i_{sc}$
	V_{3N}	i_{sb}
	V_{4N}	$-i_{sa}$
	V_{5N}	i_{sc}
	V_{6N}	$-i_{sb}$

According to their amplitudes, voltage vectors are divided into four categories: large vectors (V_{13}, V_{14}, V_{15}, V_{16}, V_{17}, V_{18}, medium vectors (V_7, V_8, V_9, V_{10}, V_{11}, V_{12}), small vectors (V_1, V_2, V_3, V_4, V_5, V_6), and zero vectors (V_0) as depicted in Fig. 2. It is significant to highlight that the voltage of the NP remains unaffected by the large and zero vectors. The small vectors, designated as V_1 to V_6, have a pronounced effect on u_o. The vector pairs influence the capacitor's voltages in opposing ways, as they can produce equivalent neutral-point current i_{np} with differing polarity. In this case, a P-type small vector (V_{1P}) is associated with an increase in u_o, in contrast to an N-type small vector (V_{1N}), which is linked to a decrease in u_o. This suggests that the impact of one redundant vector obscures the effect of the other, contingent upon the inverter's output currents being equalized. Furthermore, the neutral-point voltage is impacted by the medium vector, particularly in scenarios involving significant modulation indices or high power factors. Table 3 provides an overview of the NP current for the medium and small vector categories. By leveraging the redundancy property, one can offset the influence of the medium vector. The NP voltage achieves equilibrium when the current at the NP is zero during its active period. Therefore, the potential voltage u_o is ensured by merging the medium vector with two relevant small vectors. For instance, the neutral-point currents generated by V_7, V_{1N}, and V_{2P} correspond to i_{sb}, i_{sa}, and i_{sc}, respectively. Thus, the medium voltage V_7 can be synthesized through the combination of the negative small vector V_{1N} and positive small vector V_{2P} as:

$$
V_{M7} = \frac{1}{3}\left(V_{1N} + V_7 + V_{2P}\right). \tag{12}
$$

The established FCS-MPC necessitates 27 viable switching conditions to implement the objective function at the optimization problem's resolution. Consequently, this leads to prolonged sampling periods and significant computational demands, which can adversely affect the control system's performance. Various strategies have been offered to alleviate the computational load associated with multilevel converters. The strategies adopted a sectoral allocation of the reference inverter voltage vector, which is grounded in the space vector modulation procedure and dead-beat control [32–34]. Accordingly, the potential voltage vectors available for the 3L-NPC inverters diminish from 27 to 9, as shown in Fig. 2. Nonetheless, these approaches demand a weighting factor within the cost function to achieve equilibrium among the capacitor voltages. The challenge lies in accurately determining the ideal weighting element for specific operational scenarios, complicating the practical application in real systems. An alternative approach is introduced to alleviate the challenge of determining the optimal weighting coefficient by utilizing a suitable small redundant vector [19]. Nevertheless, this method

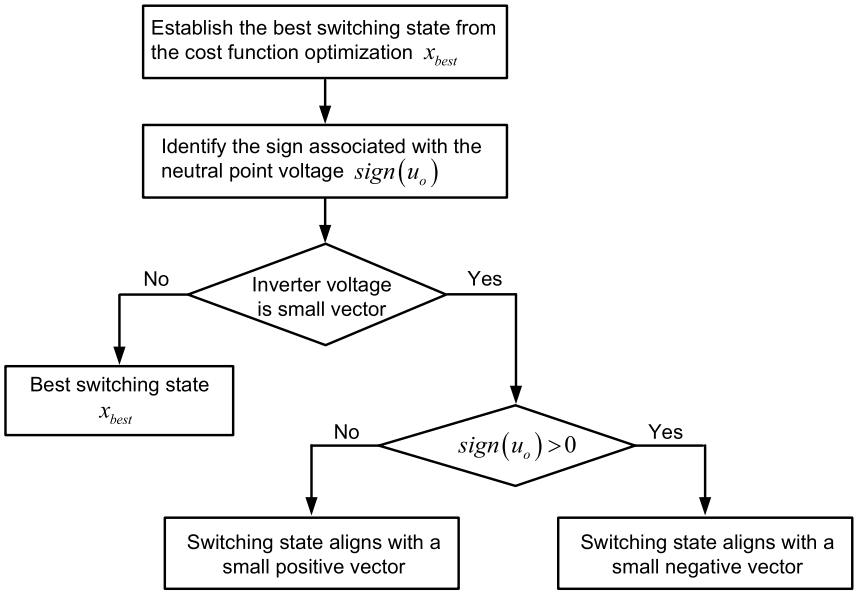

Fig. 3. Proposed technique to balance the DC-bus capacitor voltages in case of small vectors.

fails to consider the influence of medium voltage on the stability of NP voltage, particularly in scenarios involving high modulation indexes or significant power factors. The studies referenced in [9,20,28] propose an FCS-MPC strategy for virtual vector modulation in 3L-NPC inverters, which aims to counteract the effects of small and medium voltage vectors. However, this method requires complex trigonometric calculations to determine the region and the dwell time for the distribution of switching signals. To address the issues outlined, our study proposes a strategy that not only alleviates the substantial computational load but also guarantees the stability of DC-link capacitor voltages affected by medium and small vectors. Furthermore, this approach removes the requirement for selecting the most proper weighting element in the objective function. The control framework is structured around a two-phase strategy. In the preliminary phase, only the switching state of a P-type small vector is used, avoiding the two redundant small vectors that produce the same inverter voltage. The resulting neutral-point voltage imbalance is addressed through a simple condition, $sign(u_o) > 0$, which ensures the selection of appropriate switching signals. This modification reduces the conceivable switching states in the optimization objective function loop from 27 to 19. In the next step, the medium voltage vectors are accurately reconstituted to resolve the imbalance in the DC-bus capacitor voltages. For instance, using vector V_7 enables us to recalculate the inverter voltage in stationary coordinates based on two small positive and negative vectors according to (12) and (7) before applying the predictive model to estimate the stator currents. Likewise, the remaining medium voltages can be synthesized from two appropriate small vectors. These computed values facilitate the determination of the stator currents within the dq reference frame utilizing Park transformation. Table 4 summarizes the inverter voltages necessary for all medium vectors. As a result, the most suitable switching states for the PMSM, which is supplied by 3L-NPC inverters, are established by solving the optimization problem:

$$x_{best} = argmin\left\{g\left(u_{k+1}\right)\right\}, \tag{13}$$

$$\text{s.t. } u_{k+1} \in \mathbb{V} = \left\{V_1, ..., V_{19}\right\}, V_i \in \{-1, 0, 1\}^3$$

$$g(u_{k+1}) = \left\|i^*_{sd}(k+2) - i_{sd}(k+2)\right\|^2 + \left\|i^*_{sq}(k+2) - i_{sq}(k+2)\right\|^2$$

At the final stage, the optimal gate signals are implemented to the 3L-NPC inverters by integrating the most effective switching conditions from the optimization loop with the offered DC-bus voltage equalization for small vectors. Two cases are considered for the inverter voltage vector, as determined by the optimization loop: small vectors and non-small vectors. When the optimal condition corresponds to a small vector, the switching signals are generated using a straightforward control diagram, as illustrated in Fig. 3. In contrast, if a non-small vector is selected, the switching signals are directly derived from the corresponding inverter voltage vector. As an illustration, the inverter voltage identified as suitable based on the loop is V_{1P}. The perfect switching signal corresponds to V_{1N} when the NP voltage is positive u_o and the switching signal remains constant in the opposite situation. The approach presented identifies the flawless sequence of switches that matches the most reasonable inverter voltage vector. It does not require any predictions regarding the neutral-point voltage. All possible inverter voltages are computed offline before the predictive loop is initiated. Therefore, the cost function evaluations for the offered strategy are conducted exclusively for the 19 vectors in question. On the other hand, the conventional FCS-MPC method [18] requires 27 predictions of stator currents, 27 predictions of neutral-point voltages, and 27 evaluations of the objective function within each sampling duration, resulting in a significant computational cost. Additionally, this approach necessitates careful tuning of an optimal weighting factor to balance the DC-link capacitor voltages. In contrast to the previously reported approaches [9,20,28], which rely on complex calculation and modulation signals, the proposed strategy effectively mitigates the influence of medium vectors using a simple and efficient technique. Compared to the proposed method, the previous

Table 4
Required inverter voltage of medium vectors.

Medium vector	Required inverter voltage		
	Vector combination	$V_{M\alpha}$	$V_{M\beta}$
V_7	V_{1N}, V_7, V_{2P}	$V_{M7\alpha} = \frac{V_{dc}}{18}$	$V_{M7\beta} = \frac{\sqrt{3}V_{dc}}{9}$
V_8	V_{2P}, V_8, V_{3N}	$V_{M8\alpha} = 0$	$V_{M8\beta} = \frac{2\sqrt{3}V_{dc}}{9}$
V_9	V_{3N}, V_9, V_{4P}	$V_{M9\alpha} = -\frac{V_{dc}}{3}$	$V_{M9\beta} = \frac{\sqrt{3}V_{dc}}{9}$
V_{10}	V_{4P}, V_{10}, V_{5N}	$V_{M10\alpha} = -\frac{V_{dc}}{3}$	$V_{M10\beta} = -\frac{\sqrt{3}V_{dc}}{9}$
V_{11}	V_{5N}, V_{11}, V_{6P}	$V_{M11\alpha} = 0$	$V_{M11\beta} = -\frac{2\sqrt{3}V_{dc}}{9}$
V_{12}	V_{6P}, V_{12}, V_{1N}	$V_{M12\alpha} = \frac{V_{dc}}{3}$	$V_{M11\beta} = -\frac{\sqrt{3}V_{dc}}{9}$

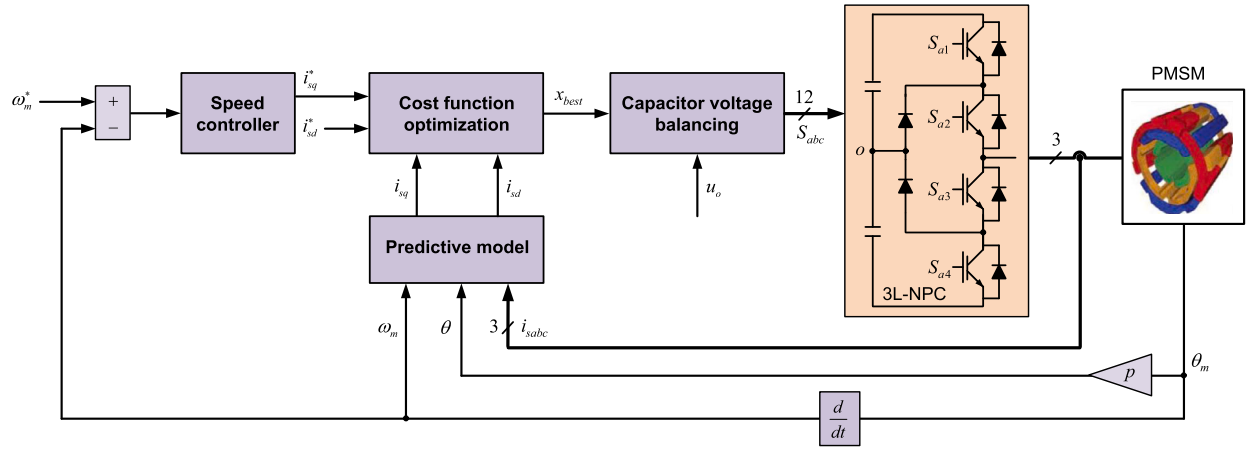

Fig. 4. Recommended diagrammatic framework for a 3L-NPC connected to a PMSM.

technique [19] uses the same number of inverter voltage vectors in the optimization loop but does not guarantee neutral-point voltage balancing due to the consequence of medium voltage vectors. This drawback can degrade control performance under such conditions. The innovative strategy presents a novel solution for streamlining computational processes while ensuring self-balance of the DC-bus voltage across various operating conditions. Additionally, a significant benefit of the offered approach is the elimination of the need to select a weighting element. Fig. 4 demonstrates the flow diagram of the enhanced control strategy. A comprehensive overview of the offered methodology is presented in Algorithm 1. Fig. 5 illustrates the flowchart of the control algorithm for both the conventional FCS-MPC method and the proposed approach.

Algorithm 1 Algorithm of the offered control strategy with self-balancing mechanisms DC-link voltage

Input: $i_{sabc}(k)$, $u_o(k)$, V_{dc}, $\omega_m(k)$, $i^*_{sd}(k)$ and $\omega^*_m(k)$
Output: Switching signal S_{abc}
Estimate the stator currents $i_{sd}(k+1)$ and $i_{sq}(k+1)$ from (8)
Compute required inverter voltage with a combination of appropriate small vector for medium vector based on (7) and (12)
Set the initial values of the best objective function g_{best} and the switching status x_{best}
for $i = 1$ to 19 **do**
  Predict the stator currents $i_{sd}(k+2)$ and $i_{sq}(k+2)$ using (9)
  Evaluate the optimization criterion $g(u_{k+1})$ from (13)
  if $g < g_{best}$ **then**
    $g_{best} \leftarrow g$; $x_{best} \leftarrow i$
  end if
end for
Identify the correct switching signals for a small vector as illustrated in Fig. 3

4. Simulation results

Matlab Simulink is utilized to conduct simulation examinations. A 3L-NPC inverter, which powers a PMSM, is constructed using Simpowersystem, with the rated parameters provided in Table 5. The speed controller operates on a PI-type mechanism, with a control sampling time of 50 μs for the FCS-MPC strategy. Nevertheless, this matter is not the principal theme of the research and will not receive additional exploration.

To confirm the effectiveness of the proposed strategy, it undergoes testing under steady-state conditions at various speeds, as well as under dynamic response scenarios involving abrupt changes in speed and load torque. An evaluative comparison is conducted on the efficiency of traditional FCS-MPC [18], model predictive current control (prior method) [19] that utilizes an appropriate small vector for DC-link voltage balancing, and the enhanced MPC introduced in this research. The evaluation

Table 5
Fundamental parameters of the investigated system.

Parameter	Symbol	Value
DC-link voltage (V)	V_{dc}	560
Capacitor (μF)	C_{dc}	500
Stator resistance (Ω)	R_s	2.875
Stator inductance (H)	L_s	0.015
Pairs	p	3
Permanent magnet flux (Wb)	ψ_m	0.175
Moment of inertia (kgm^2)	J	0.029
Viscosity coefficient (kgm^2/s^2)	B_m	0.0005

of stator current ripples is undertaken with the aid of the root mean square percentage error (RMSE), formulated as:

$$RMSE(\%) = \frac{\sqrt{\frac{1}{T_{est}}\sum_{t=1}^{T_{est}}\left(i_t - \hat{i}_t\right)^2}}{\frac{1}{T_{est}}\sum_{t=1}^{T_{est}} i_t}, \tag{14}$$

where i_t is characterized as the needed value, in contrast to $\hat{i}_t$, which is the simulated weight evaluated over the time interval of T_{est}.

4.1. Steady-state evaluation

To highlight the feasibility of the offered methodology, three scenarios were executed. Initially, the control frequency for all three schemes is established at 10 kHz. The load torque is configured to 10 Nm, while the rotor speed is set to 2000 rpm. The results at steady state for the traditional FCS-MPC, the prior approach, and the suggested technique are depicted in Fig. 6. Fig. 6 illustrates that the stator current frequency is approximately 100 Hz, with a stable speed of 2000 r/min. The d-axis current is close to 0 A, while the q-axis current measures around 12.8 A. Analyzing the current ripple, the RMSE values for the d-axis current across the standard, prior, and suggested approaches are 0.33, 0.31, and 0.32, respectively. For the q-axis current, the RMSE values are 0.27, 0.26, and 0.3 respectively. Therefore, the three control strategies exhibit slight variation in the dq-axis current ripples. The conventional FCS-MPC yields the smallest stator current ripples, as it explores all possible switching states during each optimization cycle, enabling more precise control of the output voltage. Although the proposed method exhibits slightly higher current ripples under identical sampling conditions, it offers considerable potential for enhancement. Its reduced computational complexity allows for a shorter sampling period, which in turn improves the current ripple performance. In contrast, the previous method demonstrates the poorest steady-state behavior in stator currents, primarily due to NP voltage imbalance. This imbalance arises

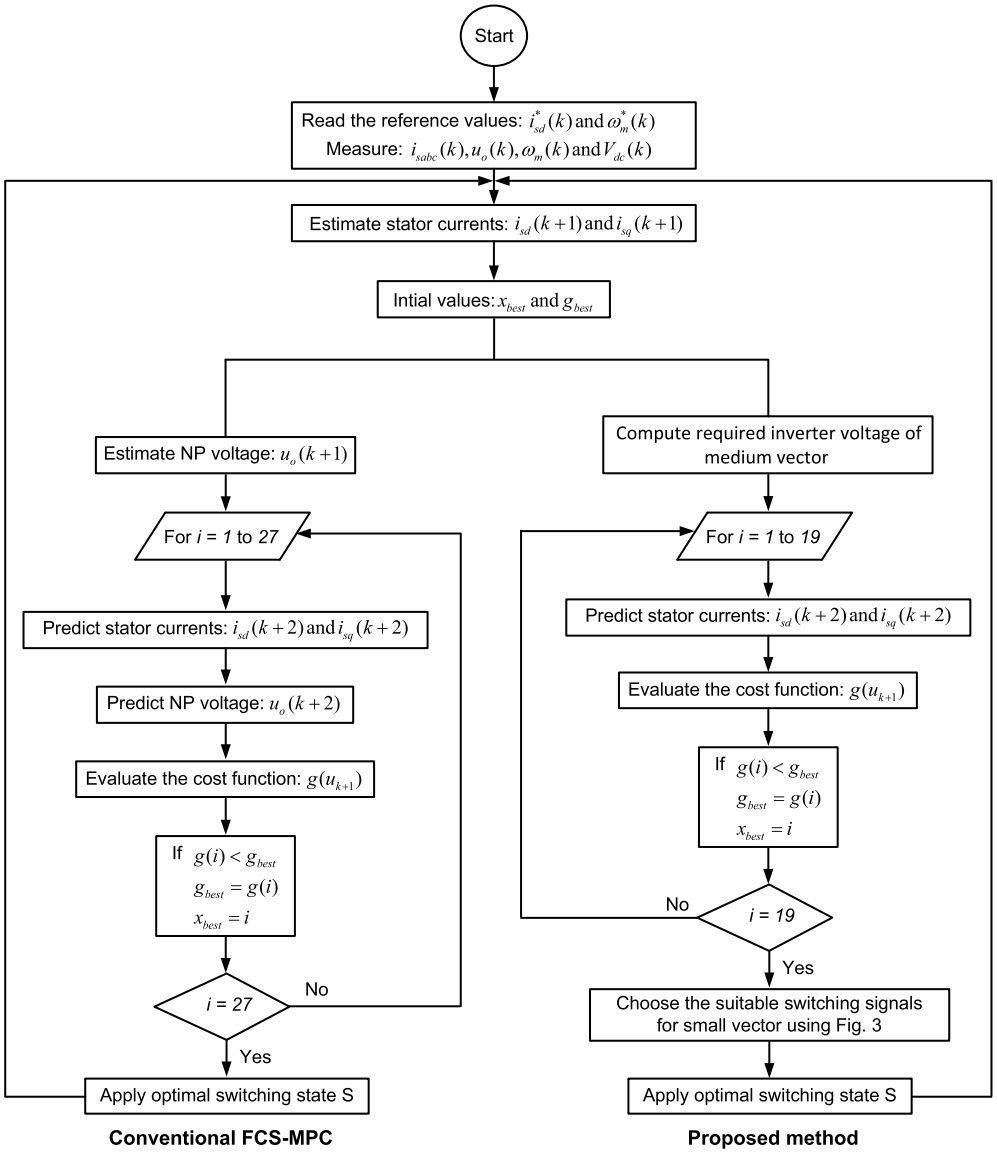

Fig. 5. Flowchart illustrating the control algorithm for both the conventional FCS-MPC and the proposed strategy.

from the use of medium voltage vectors, which fail to regulate the NP voltage effectively, leading to increased current distortion. As depicted in Fig. 6, the three control techniques demonstrate a strong ability to track the reference speed. The traditional approach has a total harmonic distortion (THD) of 0.68%, while the prior method has a THD of 0.84%, and the offered strategy has a THD of 1.03%.

To highlight the broad applicability of the strategy, a comparison of the THD among the three control techniques was performed under the same load at different speeds of 2000, 1000, and 500 rpm, as presented in Fig. 7. The suggested approach exhibits a better THD in stator current compared to the prior method during low-speed operations. This situation arises because the imbalance in the NP voltages negatively impacts the control performance of the previous technique. When evaluated against traditional FCS-MPC, the proposed technique demonstrates comparable performance, accompanied by a minor increase in THD. Although the proposed technique does not outperform the traditional approach regarding THD, it is considered to comply with the standards outlined in the IEEE 519 guideline. Additionally, its performance can be enhanced by decreasing the sampling time, which helps reduce the computational load and eradicates the requirement to select an optimal weighting factor for the optimization criterion. Fig. 8 illustrates the mechanical rotor speed and the DC-link capacitor voltage behavior for all three control techniques operating at 500 rpm. The earlier approach fails to equalize the capacitor voltages, primarily due to the influence of the medium vector voltage. This inadequacy may result in complications such as heightened harmonic distortion, diminished output quality, and the risk of damage to capacitors and switching components. In 8(f), it is evident that the voltages across the capacitors are well-balanced, with each voltage equating to half of the DC-bus voltage, facilitated by the suggested technique. This outcome affirms the design's validity and highlights the success of the suggested NP voltage balancing control.

4.2. Dynamic response

The second case explores the recommended approach by varying the rotor speed from 0 to 1500 rpm at 0.2 s, followed by a reduction to 500 rpm at 0.5 s, as depicted in Fig. 9(a). Meanwhile, the torque is increased from 0 to 10 Nm at 0.4 s. The PMSM begins from a stationary position, accelerates to 1500 rpm within 0.12 seconds, maintains that speed for approximately 0.3 seconds, and then initiates braking, with the deceleration phase lasting around 0.07 seconds. The recommended approach demonstrated remarkable speed tracking capabilities, exhibiting a rapid and seamless response that is on par with the two controllers

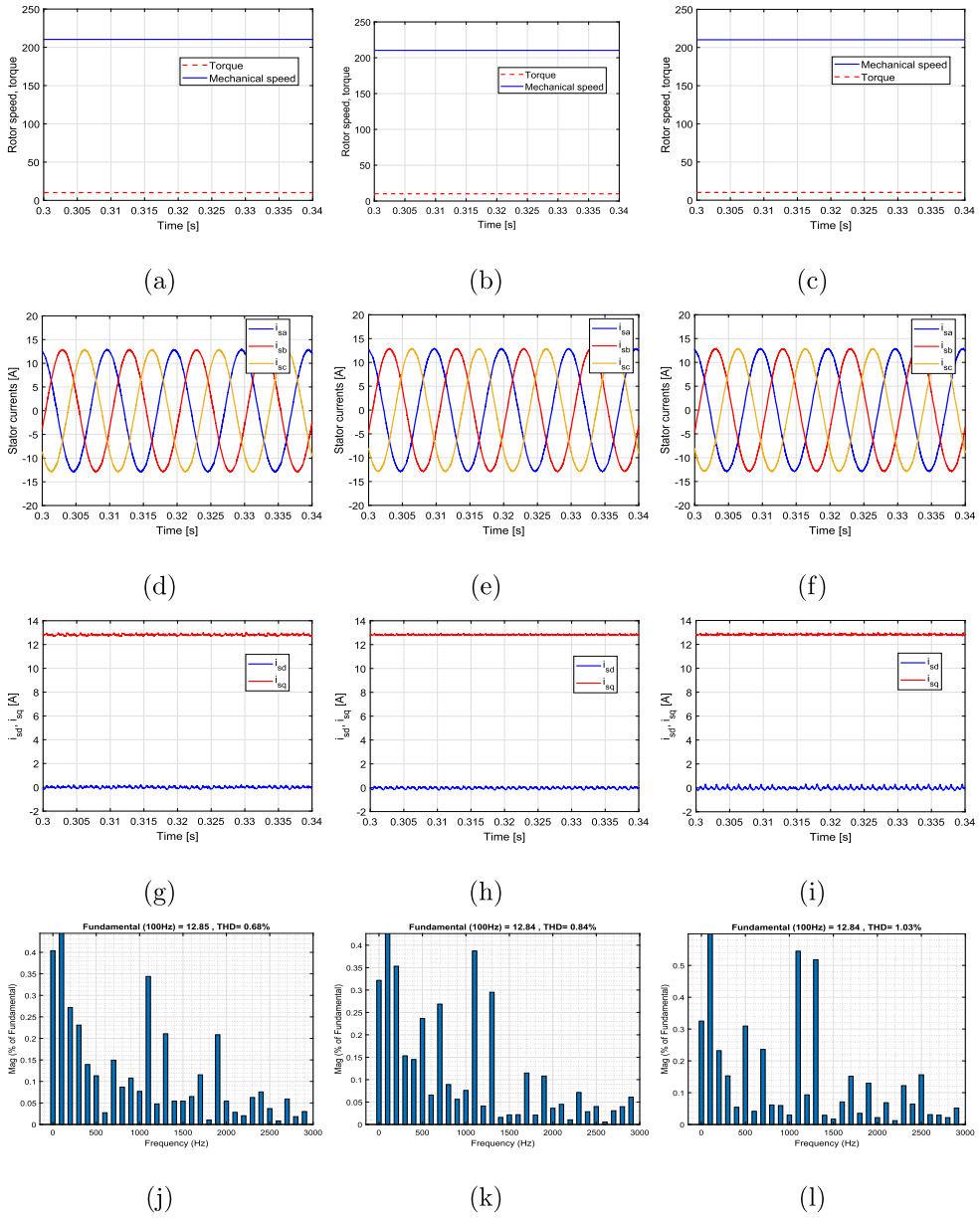

Fig. 6. Performance analysis of three control methods in a steady state: (a-c) Torque and speed of conventional, prior and proposed methods, (d-f) Three-phase stator current of conventional, prior and proposed methods, (g-i) Stator current in dq axis of conventional, prior and proposed methods, (j-l) FFT of stator current of conventional, prior, and proposed methods.

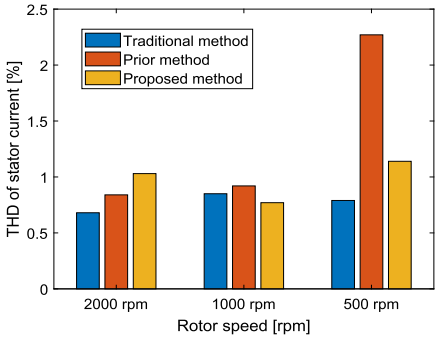

Fig. 7. Analysis of THD at various motor speeds.

illustrated in Fig. 9(b). Fig. 9(c) presents the inverter output voltage associated with the proposed method. As illustrated in Figs. 9(d), 9(e) and 9(f), the dynamic characteristics of DC-link capacitor voltages are analyzed for three methods. It is clear that the previous technique does not effectively equalize the capacitor voltages at low speeds. In contrast, the offered strategy successfully assures voltage balance among the capacitors under all operating conditions. The three-phase stator currents associated with the three control approaches are depicted at the bottom of Fig. 9(a). As the speed reference increases to 1500 rpm, the rise in stator current generates forward torque, enabling the motor to accelerate. Analysis of the dynamic results reveals that the three methods exhibit almost identical performance in terms of speed and stator currents.

The final scenario evaluates the system's response when subjected to a sudden change in torque levels. In this case, the torque rises from 0 to 10 Nm at 0.3 s and drops back to 0 at 0.4 s, while the rotor speed is held constant at 1500 rpm. As demonstrated in Fig. 10, the q-axis stator current experiences a fast reaction, while the d-axis current exhibits minor fluctuations near its reference value of 0 A. When the load is applied, the q-axis current requires 7 ms to track the reference of

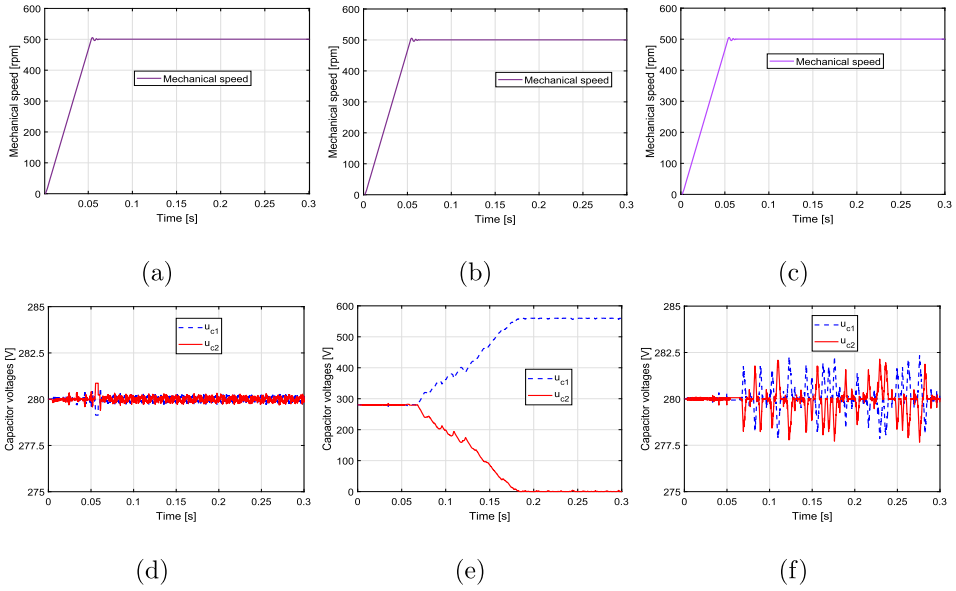

Fig. 8. Steady-state behavior of the rotor speed and DC-link capacitor voltages associated with three control strategies: (a) Rotor speed of conventional method, (b) Rotor speed of prior method, (c) Rotor speed of proposed method, (d) Capacitor voltages of conventional method, (e) Capacitor voltages of prior method, (f) Capacitor voltages of proposed method.

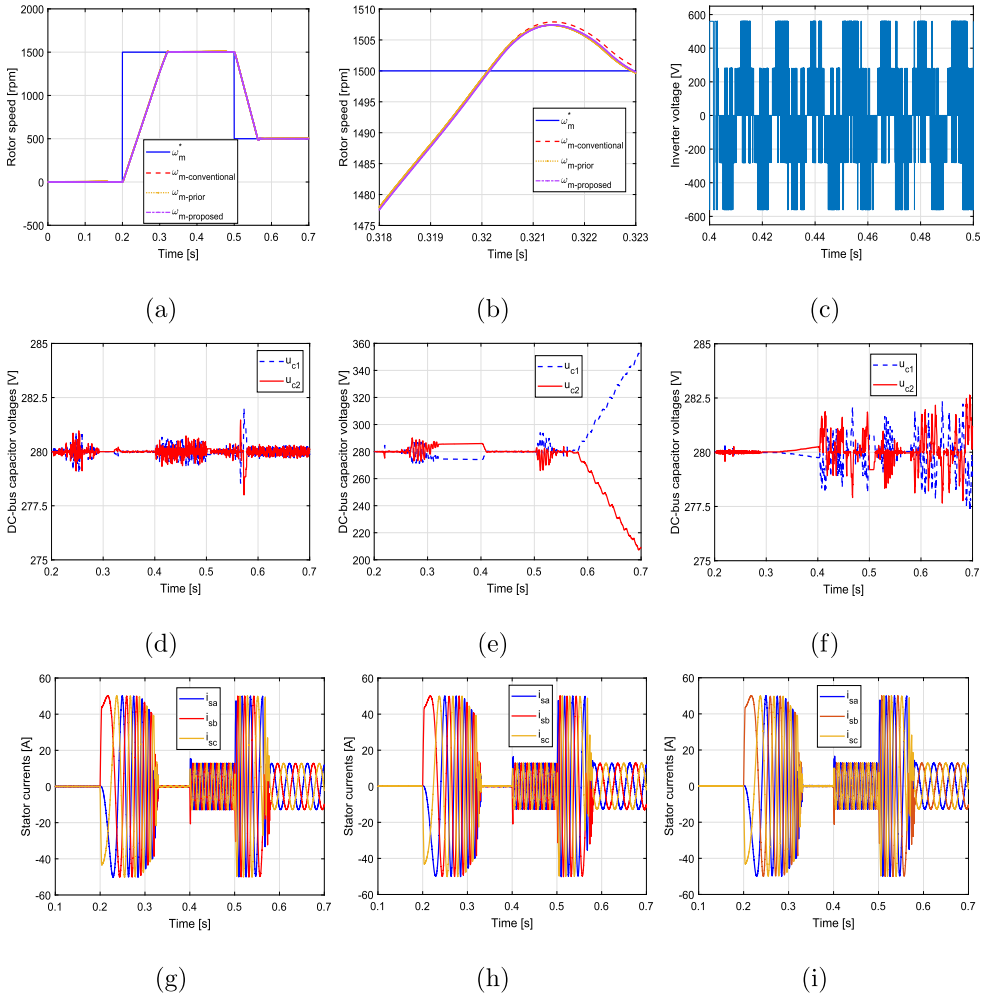

Fig. 9. Comparative performance evaluation of three control strategies under dynamic operating conditions: (a) Speed response of three methods, (b) Magnified view of speed response for the three methods (c) Inverter voltage of proposed method, (d) Capacitor voltage of conventional method, (e) Capacitor voltage of prior method, (f) Capacitor voltage of proposed method, (g) Stator current of conventional approach, (h) Stator current of prior approach, (i) Stator current of proposed approach.

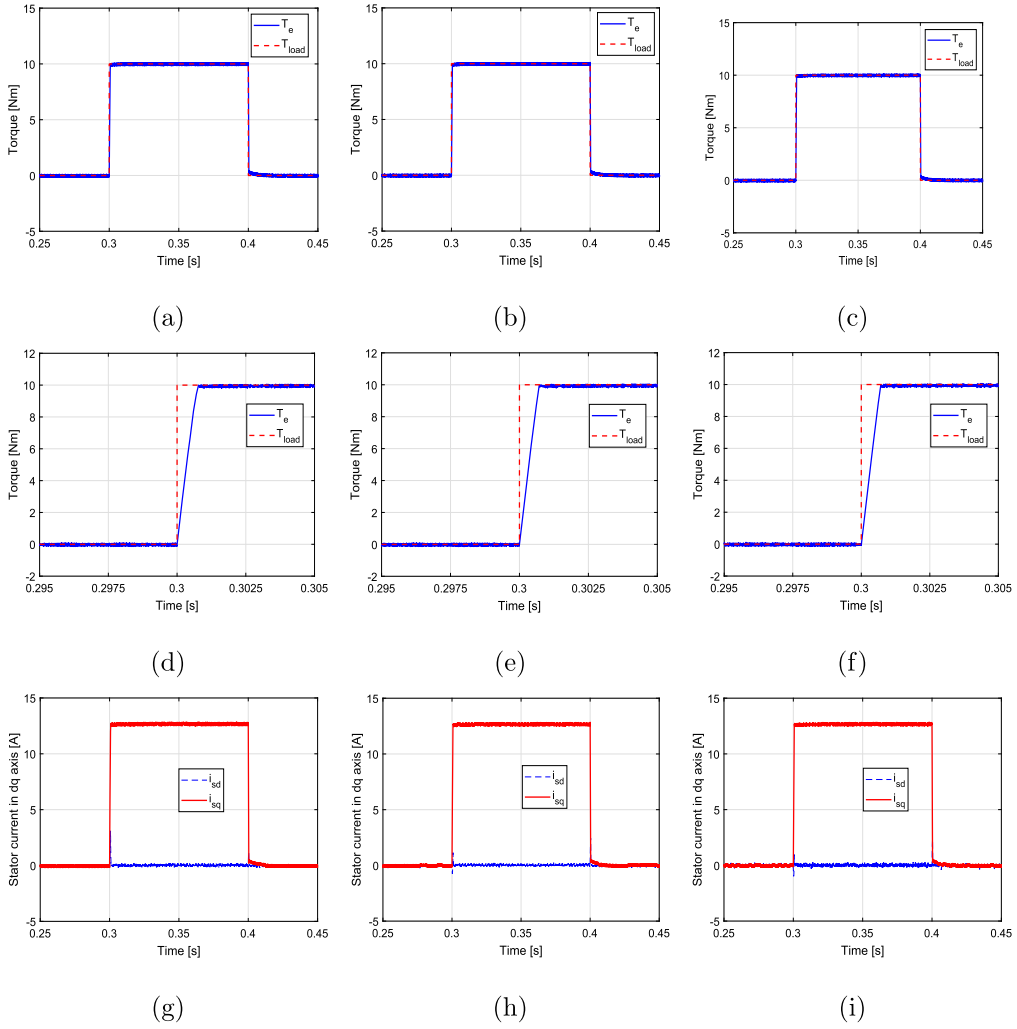

Fig. 10. Comparison of the effectiveness among three control strategies during a step change in load torque: (a) Torque of conventional method, (b) Torque of prior method, (c) Torque of proposed method, (d) Zoom of torque of conventional method, (e) Zoom of torque of prior method, (f) Zoom of torque of proposed method, (g) Stator current in dq axis of conventional method, (h) Stator current in dq axis of prior method, (i) Stator current in dq axis of proposed method.

Table 6
A performance comparison involving three different control approaches.

Mechanical speed step	$\omega_m^* = 0 \rightarrow 1500$ (rpm)		
	Conventional method	Prior method	Proposed method
Rise time (s)	0.12	0.12	0.12
Settling time (s)	0.123	0.123	0.123
RMSE of d-axis stator current (%)	0.33	0.31	0.32
RMSE of q-axis stator current (%)	0.27	0.26	0.3
THD of stator current (%)	0.68	0.84	1.03
Weighting element determination of capacitor voltages	Required	Not required	Not required
Impact of medium voltage on the capacitor voltages balancing	Considered	Not considered	Considered

12.69 A. Simultaneously, the torque from the proposed method reaches a steady state at approximately 7.2 ms. In comparison, the d-axis stator current stabilizes at 5 ms following a change in load torque from 10 to zero. The simulation results indicate that the dynamic performance of the three approaches shows negligible differences when subjected to a step change in load. Table 6 summarizes the comparative analysis of the three control methods as well as demonstrates the superiority of the proposed strategy in all motor operating scenarios.

4.3. Processor-in-loop assessment

This section outlines the use of Processor-in-loop (PIL) validation to evaluate the feasibility of the offered methodology employing a DSP controller TMS320F28379D [35,36]. The C2000 microcontroller was developed as a PIL virtual platform to support the verification of the proposed scheme and to analyze simulation results. Within this framework, the PIL setup is employed to simulate the conduct of the controlling system components-particularly the power circuit, which includes the PMSM and the 3L-NPC inverter using the SimPowerSystems toolbox. The control algorithm under evaluation is deployed on the DSP for real-time testing. Virtual serial transmission enables seamless interaction between the host system and the physical controller. The 3L-NPC inverters, associated with the PMSM, convey their measured signals to the DSP board. The controller analyzes these measured values to determine the optimal switching signals, which are subsequently transmitted back to the physical system. Fig. 11 illustrates the key features and signal paths involved in the PIL emulator for the offered strategy. Fig. 12 illustrates the results of the PIL verification for the suggested strategy. This figure depicts a scenario where the target rotor speed ranges from 500 to 1500 rpm over a duration of 0.2 seconds, while a load torque of 10 Nm is introduced at 0.4 seconds. It is evident that the suggested approach offers a quick dynamic reaction and maintains effective steady-state performance during sudden variations in speed and load. The results

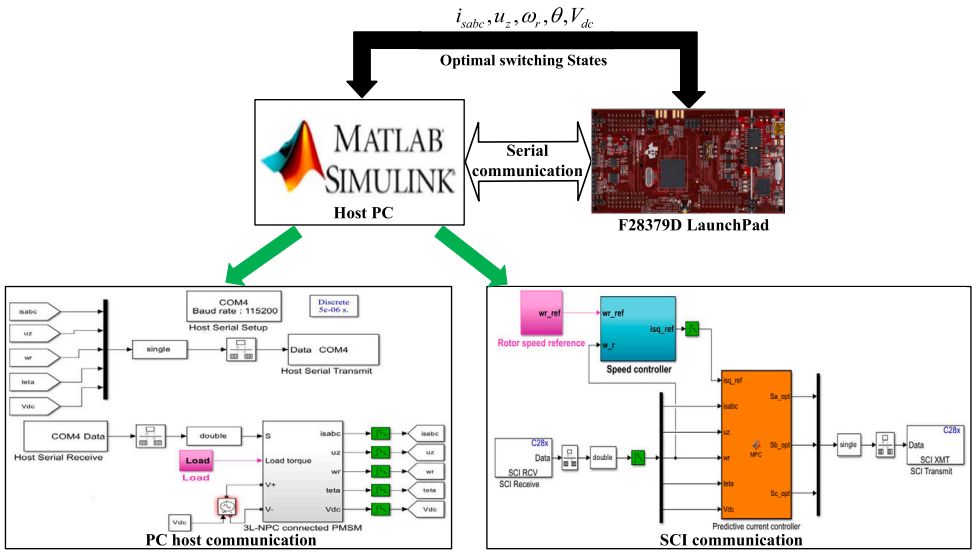

Fig. 11. The schematic representation of PIL emulator for the outlined strategy.

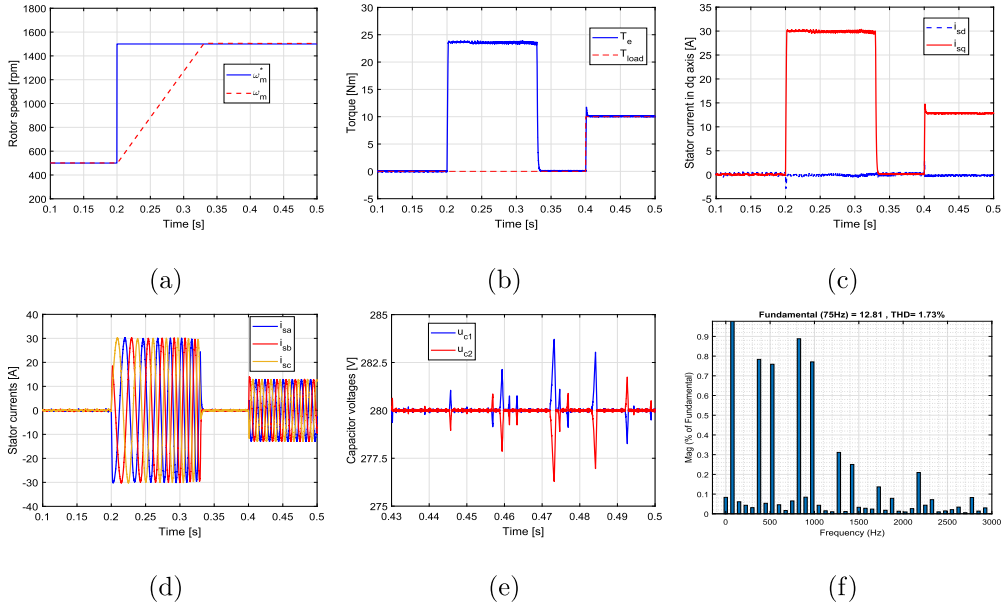

Fig. 12. The interactive response of the introduced technique assessed via PIL verification: (a) Rotor speed, (b), Torque, (c) Stator current in dq axis, (d) Stator current in abc frame, (e) DC-bus capacitor voltages, (f) FFT of stator current.

demonstrate that the THD of the stator current is consistently maintained at less than 5%. Furthermore, the DC-bus voltage remains stable throughout the operation, with the maximum observed oscillation not exceeding 6 V, as shown in Fig. 12(e). It is fundamental to recognize that the stator current signals in the dq axis obtained from the PIL setup display higher ripple levels compared to those from high-fidelity simulations. In comparison to the simulation, the RMSE of the d-axis stator current increased from 0.32% to 0.49%, while the RMSE of the q-axis stator current increased from 0.30% to 0.43%. These differences primarily stem from real-world components and limitations inherent in the PIL framework, which can introduce minor discrepancies between PIL and simulation outcomes. However, the control performance of the proposed approach can be enhanced in real systems by utilizing a more powerful processor, such as an FPGA. The strong correlation between the PIL and simulation results confirms the real-world applicability of the proposed method. This study presents a streamlined strategy for implementing FCS-MPC in 3L-NPC inverters, featuring a DC-link voltage self-balancing mechanism and reduced computational complexity. The control algorithm is implemented in a C file, making it straightforward to deploy on the DSP for real-time system operation. These findings could contribute to the development of a viable control methodology for PMSMs powered by multilevel inverters in high-power applications such as electric vehicles or industrial drives.

5. Conclusions

This research presents a scheme-oriented FCS-MPC framework for speed control in 3L-NPC inverter-fed PMSM systems. The importance of the study lies in the integration of an efficient FCS-MPC strategy designed to reduce computational complexity, ensure self-balancing of DC-link voltages, and mitigate the influence of medium voltage vectors on the NP voltage. This methodology unfolds in two distinct phases. Initially, it employs the inverter operating states of a P-type small vector. Medium voltage vectors are derived from two suitable small vectors before the rolling optimization phase, which helps to minimize computational demands through an iterative loop of 17 feasible switching

states. In conclusion, the optimal gate signals are implemented to the 3L-NPC inverter by merging the most effective switching states identified during the optimization loop with the proposed self-balancing mechanisms for small vectors. The advanced strategy delivers stable and dynamic conditions on par with conventional FCS-MPC, exhibiting similar settling times of rotor speed, current ripple, and THD of stator current, while achieving a 30% reduction in computational expenses. In contrast to the prior method, the offered algorithm ensures that capacitor voltage remains balanced across all operating conditions, including low-speed scenarios. This enhancement leads to a 49.8% reduction in the THD of the stator current from 2.72% to 1.14% at 500 rpm by effectively compensating for the influence of the medium voltage vectors. The findings of this study may support the development of an efficient and practical control strategy for PMSMs powered by multilevel inverters, especially in high-power applications such as electric vehicles and industrial drives. Future work will focus on experimentally validating the proposed method and extending it to direct model predictive speed control, with the goal of improving dynamic performance and ensuring robust operation under real-world conditions.

CRediT authorship contribution statement

Kim-Anh Nguyen: Writing – original draft, Software, Methodology. **L.D. Hieu:** Software, Project administration, Funding acquisition, Conceptualization. **Viet-Tuan Pham:** Visualization, Software, Conceptualization. **Van-Quang-Binh Ngo:** Writing – original draft, Validation, Supervision, Methodology, Investigation, Funding acquisition, Formal analysis.

Declaration of competing interest

The authors declare that they have no known competing financial interests or personal relationships that could have appeared to influence the work reported in this paper.

Acknowledgements

This paper is supported with research funding by Project code: B2024-DHH-11. This work was partially supported by Hue University under the Core Research Program, Grant No. NCTB.DHH.2025.17.

Data availability

No data was used for the research described in the article.

References

[1] P. Kakosimos, H. Abu-Rub, Predictive speed control with short prediction horizon for permanent magnet synchronous motor drives, IEEE Trans. Power Electron. 33 (2018) 2740–2750.
[2] X. Zhang, Y. Cao, C. Zhang, S. Niu, Model predictive control for PMSM based on the elimination of current prediction errors, IEEE J. Emerg. Sel. Top. Power Electron. 12 (2024) 2651–2660.
[3] Z. Zhang, X. Wang, J. Xu, Robust amplitude control set model predictive control with low-cost error for SPMSM based on nonlinear extended state observer, IEEE Trans. Power Electron. 39 (2024) 7016–7028.
[4] M.S. Hossain, N.A.M. Said, M.A. Hasan, W.A. Halim, W.N.W.A. Munim, A. Jidin, Performance evaluation of a nearest level control-based TCHB multilevel inverter for PMSM motors in electric vehicle systems, Results Eng. 25 (2025) 103949.
[5] S. Kouro, M. Malinowski, K. Gopakumar, J. Pou, L.G. Franquelo, B. Wu, J. Rodriguez, M.A. Pérez, J.I. Leon, Recent advances and industrial applications of multilevel converters, IEEE Trans. Ind. Electron. 57 (2010) 2553–2580.
[6] J. Rodriguez, S. Bernet, P.K. Steimer, I.E. Lizama, A survey on neutral-point-clamped inverters, IEEE Trans. Ind. Electron. 57 (2010) 2219–2230.
[7] I.M. Alsofyani, K.-B. Lee, Three-level inverter-fed model predictive torque control of a permanent magnet synchronous motor with discrete space vector modulation and simplified neutral point voltage balancing, J. Power Electron. 22 (2022) 22–30.
[8] G. Mayilsamy, S.R. Lee, Y.H. Joo, An improved model predictive control of back-to-back three-level NPC converters with virtual space vectors for high power PMSG-based wind energy conversion systems, ISA Trans. 143 (2023) 503–524.
[9] S. Peng, G. Zhang, Z. Zhou, X. Gu, C. Xia, MPTC of NP-clamped three-level inverter-fed permanent-magnet synchronous motor system for NP potential imbalance suppression, IET Electr. Power Appl. 14 (2020) 658–667.
[10] X. Chi, C. Wang, Q. Wu, J. Yang, W. Lin, P. Zeng, H. Li, M. Shao, A ripple suppression of sensorless FOC of PMSM electrical drive system based on MRAS, Results Eng. 20 (2023) 101427.
[11] C. Candelo-Zuluaga, J.-R. Riba, A. Garcia, PMSM parameter estimation for sensorless FOC based on differential power factor, IEEE Trans. Instrum. Meas. 70 (2021) 1–12.
[12] G. Buja, M. Kazmierkowski, Direct torque control of PWM inverter-fed AC motors - a survey, IEEE Trans. Ind. Electron. 51 (2004) 744–757.
[13] S.G. Petkar, V.K. Thippiripati, A novel duty-controlled DTC of a surface PMSM drive with reduced torque and flux ripples, IEEE Trans. Ind. Electron. 70 (2023) 3373–3383.
[14] I. Harbi, J. Rodriguez, E. Liegmann, H. Makhamreh, M.L. Heldwein, M. Novak, M. Rossi, M. Abdelrahem, M. Trabelsi, M. Ahmed, P. Karamanakos, S. Xu, T. Dragičević, R. Kennel, Model-predictive control of multilevel inverters: challenges, recent advances, and trends, IEEE Trans. Power Electron. 38 (2023) 10845–10868.
[15] H. Wang, J. Su, G. Yang, Line-constrained-based explicit model predictive current control for IPMSMs drives, IEEE Trans. Power Electron. 38 (2023) 10093–10103.
[16] S. Vazquez, J. Rodriguez, M. Rivera, L.G. Franquelo, M. Norambuena, Model predictive control for power converters and drives: advances and trends, IEEE Trans. Ind. Electron. 64 (2017) 935–947.
[17] X. Jiang, Y. Yang, M. Fan, A. Ji, Y. Xiao, X. Zhang, W. Zhang, C. Garcia, S. Vazquez, J. Rodriguez, An improved implicit model predictive current control with continuous control set for PMSM drives, IEEE Trans. Transp. Electr. 8 (2022) 2444–2455.
[18] R. Jose, G. Cristian, M. Andres, F.-B. Freddy, A. Pablo, N. Mateja, Z. Yongchang, T. Luca, D.S. Alireza, Z. Zhenbin, W. Fengxiang, N. Margarita, D. Tomislav, B. Frede, G. Tobias, K. Ralph, K.D. Arab, A. Mohamed, Z. Zhen, M. Nenad, A.R. P, Latest advances of model predictive control in electrical drives-part I: basic concepts and advanced strategies, IEEE Trans. Power Electron. 37 (2022) 3927–3942.
[19] E.E.M. Mohamed, M.S.R. Saeed, T-type multilevel inverter-fed interior PM machine drives based on the voltage regulation feedback and the model predictive control, Electr. Eng. 106 (2024) 2749–2763.
[20] X. Gu, W. Xu, G. Zhang, W. Chen, X. Jin, Three-level inverter-PMSM model predictive current control based on the extended control set, Electronics 12 (2023).
[21] F. Xiao, Z. Chen, Y. Chen, H. Liu, A finite control set model predictive direct speed controller for PMSM application with improved parameter robustness, Int. J. Electr. Power Energy Syst. 143 (2022) 108509.
[22] S. Rubino, I.R. Bojoi, E. Armando, A. Tenconi, Deadbeat direct flux vector control of surface permanent magnet motor drives, IEEE Trans. Ind. Appl. 56 (2020) 2685–2699.
[23] X. Qu, C. Peng, P. Lu, B. Ge, S. Zhang, Q. Wang, Z. Li, A three-vector model predicting torque control of permanent magnet synchronous motor with a fixed weight coefficient, IET Cyber-Phys. Syst. Theory Appl. 9 (2024) 509–520.
[24] Y. Zhang, H. Yang, Model-predictive flux control of induction motor drives with switching instant optimization, IEEE Trans. Energy Convers. 30 (2015) 1113–1122.
[25] X. Changliang, Z. Tianyi, Z. Zhanqing, Z. Guozheng, S. Tingna, Model predictive torque control with switching table for neutral point clamped three-level inverter-fed permanent magnet synchronous motor, Trans. China Electrotech. Soc. 31 (2016) 83–92.
[26] Z. Xinan, F.G.H. Beng, J. Tong, N. Tung, L.C. H. T, A simplified deadbeat based predictive torque control for three-level simplified neutral point clamped inverter fed IPMSM drives using SVM, IEEE Trans. Energy Convers. 34 (2019) 1906–1916.
[27] G.I. Orfanoudakis, M.A. Yuratich, S.M. Sharkh, Nearest-vector modulation strategies with minimum amplitude of low-frequency neutral-point voltage oscillations for the neutral-point-clamped converter, IEEE Trans. Power Electron. 28 (2013) 4485–4499.
[28] Q. Yuan, A. Li, J. Qian, K. Xia, DC-link capacitor voltage control for the NPC three-level inverter with a newly MPC-based virtual vector modulation, IET Power Electron. 13 (2020) 1093–1102.
[29] X. Chao-Qun, S. Cheng, H. Ding, M. Bing-Kui, W. Xun, Y. Tian-Jian, Improved virtual space vector modulation for three-level neutral-point-clamped converter with feedback of neutral-point voltage, IEEE Trans. Power Electron. 33 (2018) 5452–5464.
[30] Z. Zhang, C.M. Hackl, R. Kennel, Computationally efficient DMPC for three-level NPC back-to-back converters in wind turbine systems with PMSG, IEEE Trans. Power Electron. 32 (2017) 8018–8034.
[31] D. Zhou, C. Jiang, Z. Quan, Y.R. Li, Vector shifted model predictive power control of three-level neutral-point-clamped rectifiers, IEEE Trans. Ind. Electron. 67 (2020) 7157–7166.
[32] X. Liu, D. Wang, Z. Peng, Improved finite-control-set model predictive control for active front-end rectifiers with simplified computational approach and on-line parameter identification, ISA Trans. 69 (2017) 51–64.
[33] X. Liu, D. Wang, Z. Peng, An improved finite control-set model predictive control for nested neutral point-clamped converters under both balanced and unbalanced grid conditions, Int. J. Electr. Power Energy Syst. 104 (2019) 910–923.
[34] C. Zhang, C. Cen, Simplified robust two-step model predictive control for permanent magnet synchronous motor, Adv. Mech. Eng. 16 (2024) 1–12.
[35] M. Megrini, A. Gaga, Y. Mehdaoui, J. Khyat, Design and PIL test of extended Kalman filter for PMSM field oriented control, Results Eng. 24 (2024) 102843.
[36] O. Arpacik, M.M. Ankarali, An efficient implementation of online model predictive control with field weakening operation in surface mounted PMSM, IEEE Access 9 (2021) 167605–167614.